

**Self-assembled hierarchical architectures by  
liquid-phase pulsed laser ablation**

L. Yang, P.W. May, L. Yin,

Chapter 8, pp.295-314 in the book  
*Nanotechnology Research Developments*,  
ed. R. Jiménez-Contreras (Nova Science  
Publishers, New York, USA, 2008) ,

# Self-assembled hierarchical architectures by liquid-phase pulsed laser ablation

Li Yang<sup>1\*</sup>, Paul W. May<sup>1</sup>, Lei Yin<sup>2</sup>

1. School of Chemistry, University of Bristol, Cantock's Close, Bristol BS8 1TS, United Kingdom.

2. Department of Aerospace Engineering, University of Bristol, Queen's Building, University Walk, Bristol BS8 1TR, United Kingdom.

E-mail: [li.yang@bristol.ac.uk](mailto:li.yang@bristol.ac.uk)

**Abstract:** Over the past decade, liquid phase pulsed laser ablation (LP-PLA) has been used as an effective method for preparation of many nanostructured materials. This technique involves the interaction of a laser with a solid target and surrounding liquid. The laser causes the target surface to vaporise in the form of an energetic ablation plume, containing species such as atoms, ions, and clusters, travelling with high kinetic energy. These can collide and react with molecules of the surrounding liquid phase, producing new materials, often on the nanometre scale. Due the intensity of the laser and the nanosecond timescales, high temperature, high pressure, and high density conditions within the reaction volume are produced which provide a 'brute force' method of synthesising novel materials that have hitherto been inaccessible using milder, more conventional techniques. In this chapter, we discuss more recent progress in the synthesis of hierarchical, complex, and ordered crystal architectures by this novel technique. It is believed that the ability of nanostructures to self-assemble in this manner provide potential building blocks for microscale or nanoscale devices. We show that for  $C_3N_4$ , a Group IV-V covalent compound, that a range of self-assembled arrays of nanoparticles, nanorods, nanoleaf, and mesoflowers can be produced, and this also suggests that the route described here can be applicable to the synthesis of nanostructures of other similar materials. Therefore, we expect LP-PLA may play a key role in advancing complex nanomaterials into many applications in optics, electronics, biology, medicine and energy/chemical conversion.

## 1. Introduction

Although self assembly has occurred in nature for thousands of years (for instance, the formation of salt crystals and the intricate structure of snowflakes), the term ‘self assembly’ as used in chemical synthesis is relative new. Self assembly refers to the creation by physical or chemical reaction, of small building units, which may be nanoparticles (NPs), nanorods (NRs), *etc*, which then aggregate together in specific arrangements to give one-dimensional (1D), two-dimensional (2D) or even three-dimensional (3D) superstructures. [1] The aggregation may be spontaneous without human intervention, or may be as a result of changing local conditions, *e.g.* temperature, concentration, drying, *etc*. Current understanding extends only to the most rudimentary of these stages for its use in materials, biology, chemistry, and condensed matter science. [2]

Due to the emergence of a new generation of high-technology materials, 2D and 3D self-assembled, aligned superstructure materials have begun to be widely investigated over the last decade. [3, 4] It is believed that the ability of nanostructures to self-assemble with controlled crystalline orientation, size, complexity and crystal morphology provide potential applications in data storage, functional devices, communications and technology. As a result, a rapidly growing field of science has emerged to understand and control these self-organized architectures, involving the dedicated efforts of chemists, physicists, material scientists and biologists. In general, physical methods (including chemical vapor deposition [5], vapour phase transport [6], and pulsed laser ablation in vacuum [7]) and chemical methods (including hydrothermal methods [8], soft-template [9] and use of various surfactants [10, 11]) have been developed to fabricate nano- to microscale materials with a range of morphologies, such as compact hexagonal networks [12], rings [13], dandelion-shaped hollow structures [14], strips [15], tubes [16], and flower-like structures. [17] However, the former techniques require relatively high temperature, vacuum conditions, expensive equipments and sometimes complicated processes, which limit them to smaller scale fabrication. Also, conventional chemical methods usually involve the use of catalysts, surfactants and possibly complex chemical reactions, which often produce a significant amount of unwanted byproducts requiring further purification. Therefore, a technique which combines the merits of both physical

and chemical methods, while giving high yield at low cost, would be desirable, if novel self assembled materials are to be produced on an industrial scale.

One such technique, liquid-phase pulsed laser ablation (LP-PLA), has been applied to the problem of producing self-organized nanomaterials only relatively recently. LP-PLA involves focusing a high power laser beam onto the surface of a solid target, which is submerged beneath a liquid. The interaction of the laser with the target causes the surface to vaporise in the form of an ablation plume, which contains species such as atoms, ions, and clusters, travelling with high kinetic energy. The species in the plume collide and react with molecules of the surrounding liquid, producing new compounds containing atoms from both the original target and the liquid. Due the intensity of the laser and the nanosecond timescales, the instantaneous temperatures and pressures within the reaction volume can be extreme (many thousands of K at tens of GPa). [18] Such high temperature, high pressure, and high density conditions provide a ‘brute force’ method of synthesising novel materials that have hitherto been inaccessible using milder, more conventional techniques.

In this chapter, we first briefly review the use LP-PLA and its applications in synthesis of nanocrystals. Furthermore, we reported recent progress in the synthesis of hierarchical, complex, and ordered crystal architectures by this novel technique. We shall show that the chemical and physical properties of these superstructures are intrinsic to the self-assembly induced by the close vicinity of the NPs or NRs. Finally, a summary and expectation are discussed with regard to the application of LP-PLA as a synthesis route for highly desirable complex architectures.

## **2. Laser ablation of solids in liquid environments**

Pulsed laser deposition was first developed in the 1960s, shortly after the invention of the pulsed ruby laser. Since then, laser ablation in a vacuum or dilute gas has been studied by many researchers. By using different target materials and background gases, and varying parameters such as the laser wavelength, fluence, and pulse duration, it is possible to produce a wide variety of thin films. These include high temperature superconductors [19], metals, semiconductors, oxides, and other ceramics [20], and

diamond-like carbon [21]. The thin films have a variety of applications, for example semiconductor devices, electrodes, and wear-resistant coatings. [22]

The introduction of pulsed laser ablation at the solid-liquid interface was first reported by Patil and co-workers in 1987, who used a pulsed laser to ablate a pure iron target in water to form iron oxides with metastable phases. [23] Following their work, Ogale [24] extended the potential of LP-PLA for the surface modification of metals, such as metallic oxidation, nitriding, and carbiding. This pioneering work opened new routes for materials processing based on the PLA of solids in various liquids. Since then, the LP-PLA method has been used to produce a wide range of novel materials, such as nanodiamond and related nanocrystals, metallic nanocrystals, nanocrystal alloys, and metal oxides. A summary of the nanocrystals synthesized by LP-PLA is listed in Table 1.

These studies clearly indicate that LP-PLA has become a successful material fabrication technique, allowing versatile design through choosing suitable solid targets and confining liquids. Compared to the conventional methods mentioned above, the technique of LP-PLA has many distinct advantages: (i) a chemically “simple and clean” synthesis, the final product is usually obtained without byproducts and no need for further purification; (ii) low cost of experimental setup and easy controllable parameters; (iii) the extreme confined conditions and induced high temperature, high pressure region favour the formation of unusual metastable phases. A recent review by Yang [25] gives a comprehensive understanding of the nucleation thermodynamics, the phase transition, and the growth kinetics of nanocrystals by laser ablation of liquids. Therefore, in this chapter we will not discuss the effects of liquid confinement, thermodynamic nucleation and growth mechanism in detail. Instead we shall focus upon the recent progress in the synthesis of hierarchical, complex, and ordered crystal architectures by LP-PLA.

Table 1. Nanomaterials synthesis via LP-PLA in various liquids. NP = nanoparticles, NR = nanrods.

Product	Solid Target	Liquid Solution	Laser parameters
Ag NP	Ag	H <sub>2</sub> O [26, 27]	Nd: YAG laser (355, 532, 1064 nm) Laser energy: 90-340 mJ/pulse
		C <sub>2</sub> H <sub>5</sub> OH [28]	Cu vapour laser (510.5 nm) Laser fluence: 1-20 J/cm <sup>2</sup>
Au NP	Au	H <sub>2</sub> O [29]	Nd: YAG laser (532, 266 nm) Laser fluence: 5-250 J/cm <sup>2</sup>
		Alkane liquid [30]	Nd: YAG laser (532 nm) Laser fluence: 1-200 J/cm <sup>2</sup>
Co <sub>3</sub> O <sub>4</sub> NP	Co	H <sub>2</sub> O [31]	Nd: YAG laser (355 nm) Laser energy: 30 mJ/pulse
Cubic-BN NP	Hexagonal-BN	Acetone[32]	Nd: YAG laser (532 nm) Power density: 10 <sup>10</sup> W/cm <sup>2</sup>
Cubic-C <sub>3</sub> N <sub>4</sub> NR	Graphite	Ammonia [33]	Nd: YAG laser (532 nm) Power density: 10 <sup>10</sup> W/cm <sup>2</sup>
		Acetone[34]	Nd: YAG laser (532 nm) Power density: 10 <sup>10</sup> W/cm <sup>2</sup>
Diamond NP	Graphite	H <sub>2</sub> O [35]	Nd: YAG laser (532 nm) Laser energy: max 125 mJ/pulse
HfS NP	HfS <sub>3</sub>	Tert-butyl disulfide [36]	Nd: YAG laser (532 nm) Laser energy: 30-50 mJ/pulse
Mg(OH) <sub>2</sub> Tubular structures	Mg	H <sub>2</sub> O +SDS[37]	Nd: YAG laser (355 nm) Laser energy: 100 mJ/pulse
Pt/TiO <sub>2</sub> NP	Pt/TiO <sub>2</sub>	H <sub>2</sub> O [38]	Nd: YAG laser (355 nm) Laser power: 160 mJ/pulse
SnO <sub>2</sub> NP	Sn	H <sub>2</sub> O +SDS <sup>a</sup> [39]	Nd: YAG laser (355 nm) Laser energy: 100 mJ/pulse
TiO <sub>2</sub> NP	Ti	H <sub>2</sub> O	Nd: YAG laser (355 nm)
		H <sub>2</sub> O +SDS[40, 41]]	Laser energy: max 150 mJ/pulse
ZnO NP core-shell	Zn	H <sub>2</sub> O +SDS [42]	Nd: YAG laser (1064 nm) Laser energy: 70 mJ/pulse
ZnO NP	Zn	H <sub>2</sub> O [43]	Nd: YAG laser (355 nm)
		H <sub>2</sub> O +LDA <sup>b</sup>	Laser energy: max 3.2 J/cm <sup>2</sup>
		H <sub>2</sub> O +CTAB <sup>c</sup>	
Zn(OH) <sub>2</sub> layered nanocomposite	Zn	H <sub>2</sub> O +SDS[44]	Nd: YAG laser (355 nm) Laser energy: 100 mJ/pulse

<sup>a</sup> SDS is sodium dodecyl sulfate.

<sup>b</sup> LDA is lauryl dimethylaminoacetic acid.

<sup>c</sup> CTBA is cetyltrimethylammonium bromide.

### **3. Highly organized growth of carbon nitride**

To date, most nanomaterials reported to have been made by LP-PLA have been either continuous film structures, zero-dimensional (0D) NPs, or 1D NRs. Since the 0D and 1D nanocrystals can serve as building blocks in forming 2D or 3D complex architectures with long term periodic structures, it should be expected that the LP-PLA approach would have great potential as a means to grow large arrays of hierarchical, complex, oriented and ordered superstructures. Indeed, our recent findings [45, 46] indicated that the instantaneous high temperature, high pressure and high density conditions that arise when a high-intensity focused laser beam impinges upon a graphite target confined by a thin layer of liquid ammonia can promote growth of crystalline carbon nitride nanoparticles.

Carbon nitride has been the subject of numerous publications since the prediction by Liu and Cohen [47] in 1989 that crystalline  $C_3N_4$  should have superhard properties. However, successful synthesis of bulk amounts of this material still remains a challenge. Recently, we have developed two-step synthesis strategies for adding complexity to oriented nanocrystals, and shown the possibility of forming self-assembled nanostructures and microstructures of crystalline carbon nitride. This approach has involved initially using the LP-PLA process to prepare carbon nitride NP suspensions, and then sequential seeding these onto an appropriate substrate and carefully drying away the liquid. More complex nanostructures, such as observed in natural materials or biomineral 3D well-arranged architectures could also be generated [48].

#### **3.1 Nanocrystal seed preparation**

The carbon nitride nanocrystal seed solution was prepared by LP-PLA, details of which are given elsewhere. [49] Briefly, a solid graphite target (Testbourne Ltd., 99.99%) was ablated at room temperature while submerged in a 5 ml solution of 25-35% ammonia solution (Fisher Scientific, used as received without further purification) inside a sealed stainless steel cell. In order to reduce the effect of target aging, the cell was rotated at 700 r.p.m. during ablation using a standard magnetic stirrer. A Q-switched Nd:YAG laser

(532 nm, pulse duration 15 ns, frequency 10 Hz) was directed by a prism and then focused onto the graphite surface using a 25 mm-focal-length lens. The intense laser light passed through a quartz window in the top of the cell, then through ~5 mm layer of the liquid covering the graphite, to form a ~0.5 mm-diameter spot on the target surface. The ablation was typically carried out at laser fluences of 25-125 mJ / pulse for reaction times  $t = 0.5-12$  h. After ablation, a pale yellow colloidal suspension was obtained, which contained a mixture of unreacted graphite and ablation product, both in the form of NPs. The suspension was stable, with no precipitate being observed for months or even longer. The graphite sediments were filtered and removed as much as possible by boiling with 70% perchloric acid, before further characterization.

For analysis, a drop of the suspension was placed onto a transmission electron microscopy (TEM) copper grid. TEM revealed (Fig. 1a) that pristine spherical particles appeared after only 10 min ablation (laser fluence at 75 mJ per pulse, 35% ammonia) with an average diameter 15.7 nm. The size distribution (Fig.1b) was obtained from statistical analysis of Fig.1a by measuring the diameters of more than 900 particles, and fits well to a Gaussian curve. The area highlighted by the rectangle in Fig.1a indicates that some of the particles may be starting to line up. After 3 h of ablation, one-dimensional rod-like structures are formed of length ~200 nm and width 30-50 nm (see Fig.1c). Since both ends of the flat structures taper to a point, they resemble the shape of a leaf, and so henceforth have been termed 'leaf-like' structures. The inset in Fig.1c shows the selected area electron diffraction (SAED) ring pattern (obtained without any tilting) from the leaf-like nanostructures, which indicates that these structures are polycrystalline. The four inner rings, with interlayer  $d$ -spacings of 2.788, 2.256, 1.610 and 1.348 Å, respectively, were indexed as (200), (101), (211) and (221) with reference to the calculated structure for  $\beta$ -C<sub>3</sub>N<sub>4</sub> ( $a = 6.4017$  Å,  $c = 2.4041$  Å, space group: P6<sub>3</sub>/m (176)) [50,51], which are identical to that reported in the literature for the same  $\beta$ -C<sub>3</sub>N<sub>4</sub> crystal. [52]

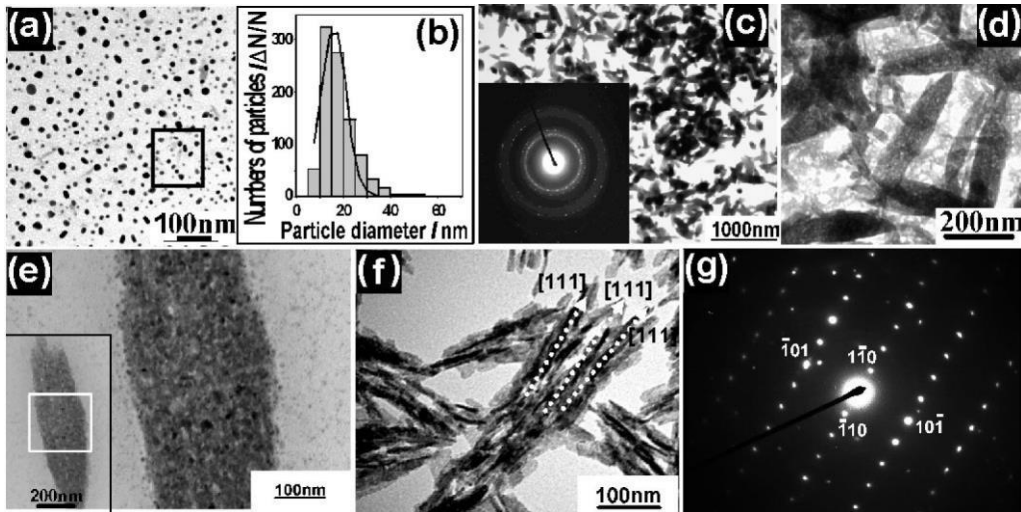


Figure 1: TEM images of  $C_3N_4$  nanostructures synthesized with 5 ml 35% ammonia covering a graphite target, using 75 mJ / pulse laser fluence. (a) After 10 min ablation, spherical NPs appear, with an average size of 15.7 nm. Adjacent particles are aligned with one another along their main axes, highlighted by the rectangle. (b) Size distribution of the NPs, with a Gaussian fit to the data. (c) Overall appearance of the leaf-like nanostructures after 3 h ablation. Inset shows a typical SAED pattern taken from Fig.1c. (d) Leaf-like structures of length  $\sim 500$  nm produced following 5 h ablation time. (e) A single leaf-like unit formed from numerous small NPs (inset area framed with white box). (f) The NR aggregates exhibit a long-range order; arrows indicate the projecting direction along [111]. (g) A SAED pattern of a NR from the [111] zone-axis indicating the area is single crystal and consistent with crystalline  $\beta$ -carbon nitride. (Reproduced from [45] by the permission of American Chemical Society (ACS))

When the reaction time was increased to 5 h (Fig.1d) the size of nanoleaf structures increased to  $\sim 100 \times \sim 500$  nm. The high magnification TEM image (Fig.1e) from a single nanoleaf shows that these structures are, themselves, composed of a large number of smaller NPs that have close-packed together in an ordered arrangement to form the leaf-like shapes. In contrast, Fig.1f shows that these leaf-like nanostructures are mostly made up of component NRs, while NPs are the building blocks for the NRs. These tiny NRs are well-aligned and all point in the same direction, perpendicular to the propagating  $c$ -axis. Although individual leaf-like structures within a local region seem to be randomly oriented, the overall NR aggregates still exhibit long-range ordering [53] (Fig.1f). A representative SAED pattern is given in Fig.1g, showing diffraction spots

from the  $(\bar{1}10)$ ,  $(\bar{1}\bar{1}0)$ ,  $(\bar{1}01)$  and  $(10\bar{1})$  planes of the  $[111]$  zone-axis, which are aligned parallel each other.

### 3.2 Chemical bonding environment in carbon nitride

X-ray photoelectron spectroscopy (XPS) measurements estimated that the overall elemental composition of the nanoleaf structures (laser fluence at 100 mJ per pulse, 35% ammonia) was 86.3% C, 11.4% N, and 2.3 % O after 5 h, whereas for 7 h ablation values were 90.5% C, 7.8% N and 1.7% O. One possibility for the presence of the O signal is that the graphite target reacted directly with the water (or OH radicals generated in the water) during the high temperature conditions in the ablation plume. However, since the O signal decreased with longer ablation time, this idea has been discounted. An alternative explanation is that prolonged exposure of the samples to the laboratory atmosphere led to possible contamination by absorbed or adsorbed water vapour. For pure  $C_3N_4$ , we would expect a composition of 42.8% C and 57.2% N, which shows that our samples are considerably carbon rich. Since we know from TEM observations that regions of the samples contain pure  $C_3N_4$ , we must conclude that our samples are a composite of crystalline  $C_3N_4$  and an amorphous carbon background. This observation is consistent with the conclusions by other workers [54, 55], who found that it was difficult to generate highly ordered structures containing large concentrations of N incorporated into the C network.

The breadth and asymmetry of the C ( $1s$ ) and N ( $1s$ ) core-level XPS spectra shown in Figure 2 indicate the presence of different bonding states within the crystallites. The core-level lines were fitted to the Gaussian function. [56] The N  $1s$  feature is difficult to assign unambiguously, since it is known that N can give a broad XPS peak around 399 eV in some materials. Alternatively, a better fit can be achieved if the feature is deconvoluted into three peaks (as shown in Figure 6), located at  $\sim 398.5$  eV,  $\sim 399.6$  eV and  $\sim 400.2$  eV, respectively. The peaks situated at  $\sim 398.5$  eV can be assigned to  $sp^3$  C-N bonds, and one at 400.2 eV assigned to  $sp^2$  C=N bonds. [57] A peak centred at a binding energy  $\sim 399.6$  eV has been assigned by some groups [58, 59] to N atoms bonded to  $sp$ -hybridized C atoms (*i.e.*  $-C\equiv N$ ). These assignments are also supported by *ab initio*

binding-energy calculations. [60] Nevertheless, within experimental accuracy it is impossible to distinguish between these two alternatives. Also, it should be noted that  $C\equiv N$  bonds can produce 3 peaks in this region [59], 398.2 eV [61], 398.1 eV [62] and 400.1 eV. [63] However, these assignments have been discounted since they are outside of the experimental accuracy of the XPS spectrometer. The presence of  $sp^3$  C-N in the ablated nanostructures is, again, in agreement with a  $C_3N_4$  structure.

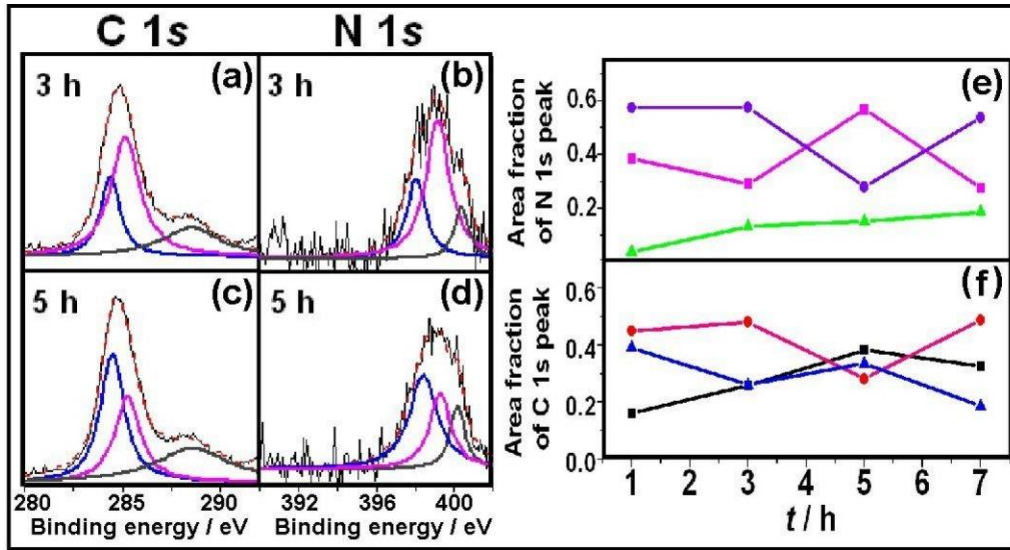


Figure 2. XPS spectra of  $C_3N_4$  nanostructures (laser fluence at 100 mJ per pulse, 35% ammonia) for different ablation times  $t$  (a) C (1s) 3 h ; (b) N (1s) 3 h; (c) C (1s) 5 h; (d) N (1s) 3 h. Each spectrum has been deconvoluted by fitting to three Gaussian lineshape functions, with the total fitted line overlaid as a dashed line. Plots showing the time dependencies of the relative areas of the Gaussian functions used to fit (e) the N (1s) XPS peak (key:  $\blacksquare$  398.5 eV  $sp^3$  C-N bonds,  $\bullet$  399.6 eV  $C\equiv N$  bonds,  $\blacktriangle$  400.2 eV  $sp^2$  C=N bonds), and (f) the C (1s) XPS peak (key:  $\blacksquare$  284.6 eV,  $\bullet$  285.5 eV,  $\blacktriangle$  288.5 eV). (Reproduced from [49] by the permission of Institute of Physics (IOP))

Similarly, the C 1s core-level spectra obtained by XPS (Figure 2) was deconvoluted into three peaks located at  $\sim 284.6$  eV,  $\sim 285.5$  eV and  $\sim 288.5$  eV, respectively. However, unlike nitrogen, verification of the assignment by independent C (1s) spectra was relatively difficult due to small shifts in binding energy and multiple bonding environments of the carbon. Carbon atoms may have zero, one, two, or three bonds with nitrogen atoms, which complicate the situation, so that there is a wide range

of interpretation in the literature for carbon spectral feature identification. The peaks at  $\sim 284.6$  eV and  $\sim 285.5$  eV can be identified unambiguously as  $sp^2$  and  $sp^3$  hybridized carbon [64, 65]. But the assignment for the peak at  $\sim 288.5$  eV has not yet reached a consensus. In our case, it is believed this peak corresponds to  $N\equiv C$   $sp$  bonding [63] supported by the Raman data. [49] Le Normand *et al* [66] have claimed that it is inappropriate to assign components appearing at higher energies to specific C-C or C-N bonding environments. After searching a comprehensive range of organic polymers, Beamson and Briggs [67] also found that no significant difference in C 1s position can be appreciated between  $sp^2$  and  $sp^3$ -hybridized carbon bonded to nitrogen.

The relationship between ablation time and relative peak area fraction is shown in Fig. 2e. The peak area corresponding to C=N ( $sp^2$ ) bonding indicates a marked increase with prolonged ablation time, whereas the trends for C $\equiv$ N ( $sp$ ) and C-N ( $sp^3$ ) are relatively complex. Nitrogen inclusion into the CN network changes the shape and position of the C 1s peak, as seen as in Fig. 2f. However, only the signal attributed to C=C ( $sp^2$ ) bonding shows smooth variation, *i.e.* increasing with ablation time, while all other signals show a more complicated trend.

### 3.3 Control of self-assembled structures

To understand the formation mechanism of nanocrystalline carbon nitride, experiments were performed for different laser energies with constant ablation time (3 h) and ammonia concentration (35%). Figure 3 summarises the different  $C_3N_4$  nanostructures synthesized with varying laser fluences. For low laser fluence (25 mJ/pulse), the leaf-like structures had a length and width of  $\sim 300$  and  $\sim 120$  nm, respectively, with smooth surfaces, and were composed of smaller-sized NPs (Fig.3a). There were also plenty of voids situated between some of the NRs (Fig.3b). The sharp SAED pattern for the leaf-like structures (inset Fig.3b) was consistent with crystalline hexagonal  $\beta$ -phase carbon nitride. [51,68] When the laser power was increased to 50 mJ / pulse, the aligned leaf-like structures increased to a length and width of  $\sim 600$  and  $\sim 250$  nm, respectively (Figs.3c-d), and now consisted of a substantial number of connected NRs, although there was no apparent change in size of the component NRs.

The surface of the leaf-like structure was no longer smooth, but contained numerous protruding NRs. For still higher fluences (75 mJ / pulse), there was no further significant change in the size or shape of the leaf-like structures and NR building units (Fig.3e-f), but there was an increase the number formed. With further increases in fluence to 100 mJ per pulse, micron-scale carbon nitride spheres (Fig.3g) were observed, which were formed following aggregation of a large number of the leaf-like structures. ‘Flower-like’ spiked crystallites (Fig.3h) were also seen, where the leaf-like structures coalesced at a common centre with multi-fold symmetry. [14] In general, the trend is that the size of the overall nanocrystallites and their basic building blocks increases with increasing laser power.

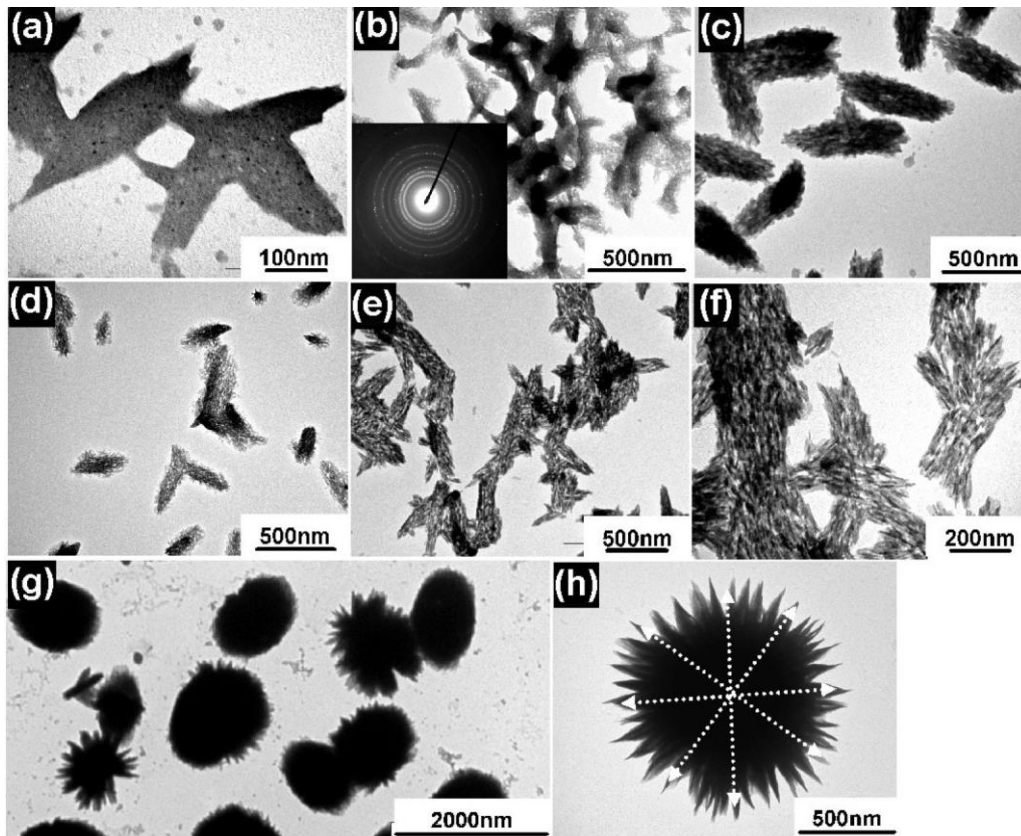


Figure. 3 TEM images of  $C_3N_4$  nanostructures synthesized for 3 h ablation time and 35% ammonia solution using different laser fluences. (a) and (b) 25 mJ/ pulse, leaf-like structures containing spherical NPs and short nanorods. Inset in (b) is a sharp SAED pattern indicating the structures are crystalline. Note that there appear to be voids inside the leaf-like structures (the white areas in the grey area of image (b)). (c) and (d)

50 mJ/ pulse, denser leaf-like structures containing longer NRs which protrude from the surface. (e) and (f) 75 mJ/ pulse, leaf-like structures beginning to aggregate into larger clumps. (g) and (h) 100 mJ/ pulse, carbon nitride nanospheres and flower-like spiky crystallites. (Reproduced from [45] by the permission of American Chemical Society (ACS))

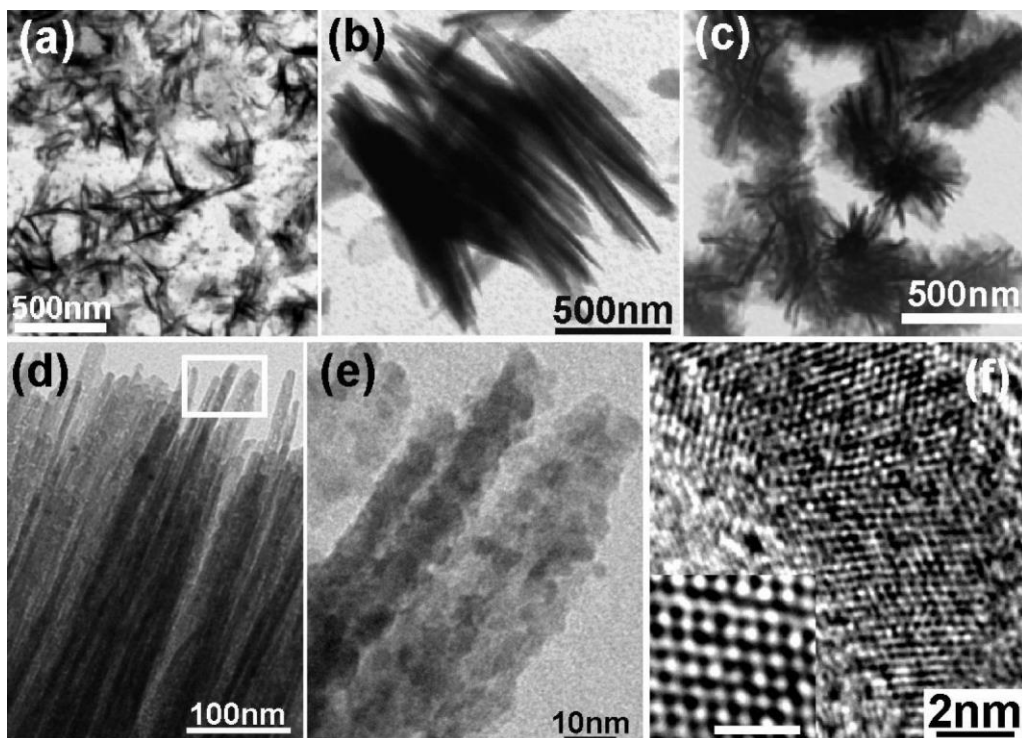


Figure. 4 TEM images obtained by LP-PLA in 25% ammonia solution: (a) isolated carbon nitride NRs (40 mJ/ pulse,  $t = 1$  h) (b) Branched NRs (40 mJ/ pulse,  $t = 3$  h) (c) highly branched flowerlike architectures (100 mJ/ pulse,  $t = 12$  h). (d) Rod-like structures showing straight, long and sharp tips. (e) Enlarged image of the region at the top of the NRs indicated by the open box in (d). (f) HRTEM image of a single NR, the inset shows the atomic arrangement.

When 35% ammonia was replaced by 25% ammonia solution, carbon nitride was still formed on the copper grids; however, the morphology was different, as mentioned previously. For low laser power (40 mJ) and short ablation time (1 h), the product contained mostly a sparse collection of isolated NRs (Fig. 4a). With longer ablation times (3 h), the NRs start to aggregate into branched structures (Fig. 4b), serving as the starting points (or nucleation seeds) for the subsequent growth. However, with increasing laser power (100 mJ) and ablation time (12 h), the concentration of NRs increased, highly

branched flower-like architectures completely made up of NRs can be observed (Fig. 4c). The NRs at the edge of the flower structures appeared to be protruding outward by  $\sim 10$  nm. As shown in Fig. 4d-4e, it should be pointed out that these NRs are themselves composed of a large number of smaller NPs that have packed together in an ordered arrangement to form the rod-like shapes. In particular, in the high-resolution (HR) TEM image in Fig. 4f, taken from a single NR, the periodic lattices clearly show the atomic arrangement (Fig. 4f inset) with very few defects, and reflect the relationship between the orientation of the NPs and the crystallography of the ordered NR array.

Based on above discussion, it was found that the size and morphology of the ablation products were a complicated function of laser power, ablation time, and ammonia concentration. Different experimental conditions can be used to optimize and control the nanocrystals nucleation and orientation independently.

#### **4. Sequential nucleation and growth of complex nanostructures**

The fabrication of well-defined 2D and 3D nanostructures is usually difficult because control of the nucleation and growth is still a challenge. Complex architectures are normally related to multistep syntheses, which begin with substrate surface preparation for heterogeneous nucleation of oriented nanocrystals. Two basic approaches have been used: one is deposition on chemically modified interfaces using organic self-assembled monolayers (SAMs). [69] Another, more straightforward method, is to seed the substrate with NPs of the desired film material. [70]. The fundamental advantage of seeded growth is enhanced control, obtained by separating the NP film nucleation and oriented rod growth into two steps.

Extending this concept, we performed a two-step synthesis to produce oriented carbon nitride nanostructures. Much more complex nanostructures than simple NPs and NRs (see the former section) can be produced in a controlled fashion by simply altering the drying time and drying method of the suspension of ablated product. In this methodology, the carbon nitride materials produced in initial LP-PLA step was physically deposited onto a silicon p-(100) substrate, and then the liquid removed by drying. Four different drying processes were used: (1) dry naturally in air; (2) dry in a sealed tube; (3)

dry in an oven or hotplate; (4) dry in a critical point dryer (CPD). CPD is a widely used drying technique in which the surface tension can be reduced to zero during evaporation. [71] Those procedures allowed the time taken to evaporate the liquid to be controlled.

#### 4. 1 General structural features

By drying the suspension under different conditions, four main classes of structure have been identified in the ablation product, categorised based upon their shape and size (Fig. 5a). The first class of structure had the shape of thin plates with rounded edges. Since they were the components of the larger ‘flower-like’ structures (described later), they have been termed ‘nano-petals’. The quantity of these nanopetals and their location with respect to the larger structures (see later) were dependent upon the deposition and drying conditions. As shown in Fig. 5b-5c, this indicated that these nano-petals were 2D aligned crystallites carbon nitride which preferentially aligned themselves perpendicularly to the surface of the Si substrate. The number and length of these nano-petals increased with increasing laser ablation time from 0.5-2 h for the same laser fluence. It is also possible that these nano-petals began to aggregate and self-assemble (Fig. 5d). When the concentration of nano-petals in the suspension increased, they try to minimize their interfacial energy upon subsequent drying of the liquid by preferential tilting with respect to each other. This produces the second class of nanostructure, which has a ‘grass-like’ shape and exhibits several different morphologies (see later). However, all are produced in large quantities and cover the whole substrate.

By carefully controlling the drying process, ‘flower-like’ spiked, crystalline superstructures were formed (Fig. 5e-5f). This third class of structure, now fully 3-dimensional, with sizes 1-20  $\mu\text{m}$ , were created when many nano-petal structures coalesced at a common centre with multi-fold symmetry. One possible explanation is that the presence of the solid substrate physically hinders growth in that direction; so many branches are tilted away from the substrate, towards the solution.

When the evaporation speed of the liquid was rapid (for example, drying in an oven or hotplate), a fourth class of structure was observed (Fig. 5g-5h). Instead of 3D flowers, the carbon nitride now formed 2D ‘star-like’ or flattened flower-like structures.

New dendrites emanated from the core and acted as nucleation centres, eventually allowing the structure to expand into 2D horizontal flowers (Fig. 5h). It is suggested that the higher water evaporation rate increases the interparticle capillary forces. [72] As the continuous flux of particles fill up the spaces on the substrate, successive layers are expected to be formed rather than 3D complex shapes.

Although these four kinds of structures have different densities and morphologies, they all exhibit high surface-to-volume ratio and so might have potential in semiconductor devices, anticorrosion protective coatings and new applications.

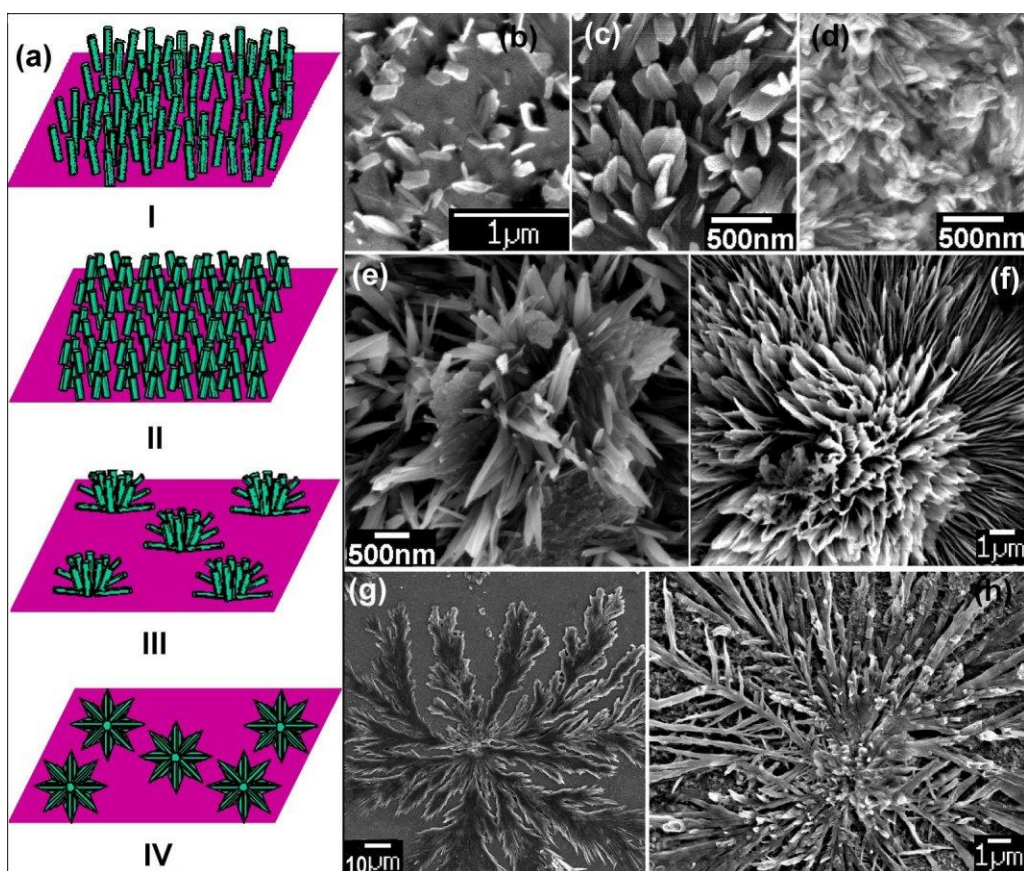


Figure.5: (a) Schematic illustration of the growth process leading to the observed four main classes of hierarchical structures, (b)-(e) SEM images of carbon nitride ‘nanopetals’ following ablation times of: (c) 0.5 h, (d) 2 h, and (e) 3 h. (e-f) Overall ‘flower-like’ structure following 5 h laser irradiation (synthesis conditions: laser power 125 mJ, 35% ammonia solution, drying in air). (g-h) 2D flattened flower, sample conditions identical to (e-f) except it was dried on a hotplate at 200°C (g) and an oven 80°C (h). (Reproduced from [48] by the permission of Royal Society of Chemistry (RSC))

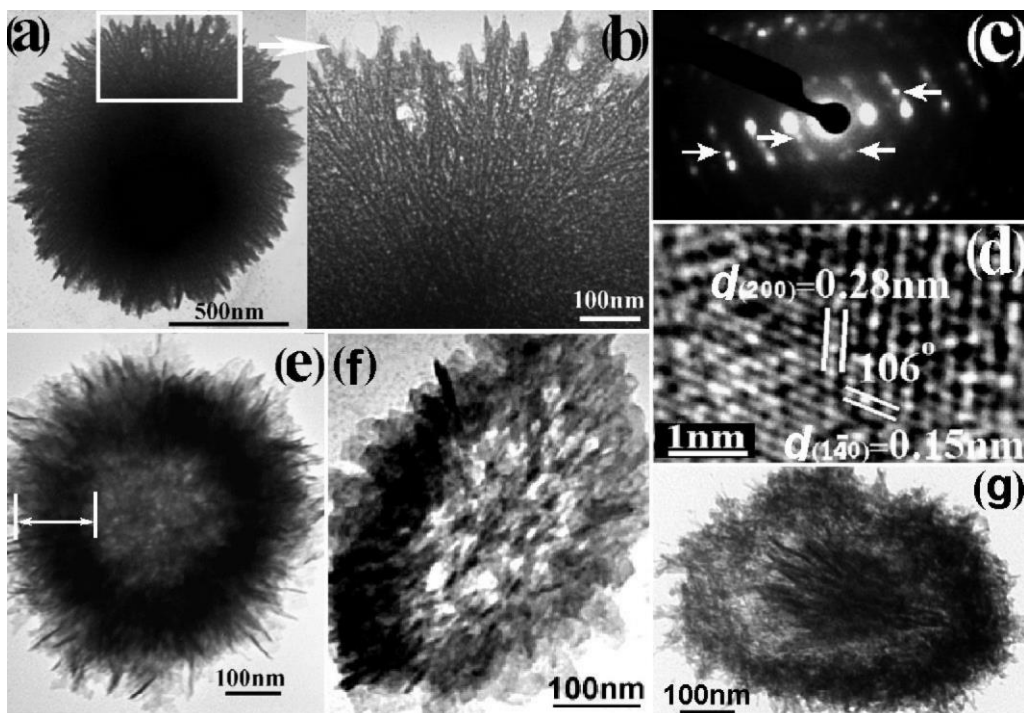


Figure. 6: (a) TEM image of the flower-like structures produced by LP-PLA of a graphite target in 35% ammonia solution (laser fluence 125 mJ/pulse) for 5 h. (b) A higher magnification image of the framed region in (a), showing a high density of NPs surrounding the nano-petal framework. (c) [001] zone-axis MDA pattern from the tips of the nano-petals in (b), which corresponds closely to the calculated interlayer  $d$ -spacing of  $\beta$ -C<sub>3</sub>N<sub>4</sub>. Arrows point to different sets of [001] reflections (see text). (d) HR-TEM image recorded from the edge of the flower nanostructure that is oriented along [001]. (e) TEM image of a hollow flower formed after 8 h LP-PLA and prolonged drying. (f) Semi core-shell structure. (g) core-shell structure with a hollow tunnel. (Reproduced from [48] by the permission of RSC)

Fig. 6a shows a symmetric carbon nitride ‘flower’ together with its nano-petal building blocks (which look like flattened rods in the TEM). Fig. 6b shows that these nano-petals appear fused together and ‘interwoven’ to form a lattice-like framework of the flower-like superstructure. The figure also shows the NPs that surround each nano-petal, and which fill in the holes within the framework to produce a dense, solid structure. Energy-dispersive X-ray (EDX) analysis confirms that carbon and nitrogen are present in all these structures, and micro diffraction analysis (MDA, Fig. 6c) was also consistent with crystalline hexagonal  $\beta$ -phase carbon nitride oriented along the [001] zone-axis. Several [001] patterns in Fig. 6c can be identified at the same time, indicating that the nano-petals consist of several domains, with different rotational orientations contributing

to the diffraction pattern. The HR-TEM image in Fig. 6d shows that the nano-petals at the very edge of the flower contain very few defects and are single crystalline, as was anticipated from the MDA pattern. Again, the lattice fringes ( $d_{200} = 0.28$  nm,  $d_{140} = 0.15$  nm) and their angles ( $106^\circ$ ) are in good agreement with the calculated values for hexagonal  $\beta$ - $C_3N_4$ . [73]

The smaller NPs, which lie in and around the nano-petal-framework comprising the flowers, appeared to be mobile with respect to this framework, and diffused outward from the centre of the flower with longer drying times. The results of this diffusion can be seen in Fig. 6e, where the solid carbon nitride flower (similar to that in Fig. 6a) has become hollow. The NPs have diffused from the centre but remain loosely attached to the outside, making the outer shell of the flower appear fuzzy. The thickness of the fuzzy shell was  $\sim 140$  nm and that of the hollow core was  $\sim 200$  nm (shown as a lighter colour in the image). When the suspension was placed onto a hot-plate at  $200^\circ\text{C}$  for 0.5 h, the hollowing process was accelerated to form a semi-core-shell structure. The radial distribution of the NRs formed channels leading from the centre to the shell (Fig. 6f). Another type of hollow structure was observed when the core-shell structures were essentially separated by a hollow tunnel, without linkage to the sphere (Fig. 6g).

## 4. 2 Arrangement of components among the architectures

The assembly process of hierarchical nanocrystals by repeated nucleation and growth is illustrated in Fig. 7. By careful observation, it was found that the mesophase flower has a symmetry structure (Fig. 7a), consisting of lots of 2D radial nanopetals and radial growth from a central nucleus. [74] In addition, each nanopetal is constructed from many tiny nanocrystals or NR subunits (Fig. 7b), as seen at the edge of the nanopetals (also see the later discussion). Surprisingly, just as for the nano-petals mentioned earlier in Fig. 6b, these NRs also appeared to be ‘interwoven’ together into a similar lattice-like framework (Fig. 7c). Interestingly, the NPs or NRs can self-assemble into a petal-like architecture along the  $c$ -axis direction. The tiny NPs attached side-by-side and fuse into the wall of the nanopetal. This has the effect of making the nanopetals surface rough and curved, and can even make the two ends join together to form tubes (Fig. 7d). Some

nanopetals also revealed structures inside the tubes, see the highlighted arrows in Fig. 7d-f. The inset of Fig. 7f shows a primary subunit with size of about 20 nm. It is worth pointing out that the length of the nanopetals is in range of 1-20  $\mu\text{m}$ , while the sizes of the subunit NPs or NRs have barely changed.

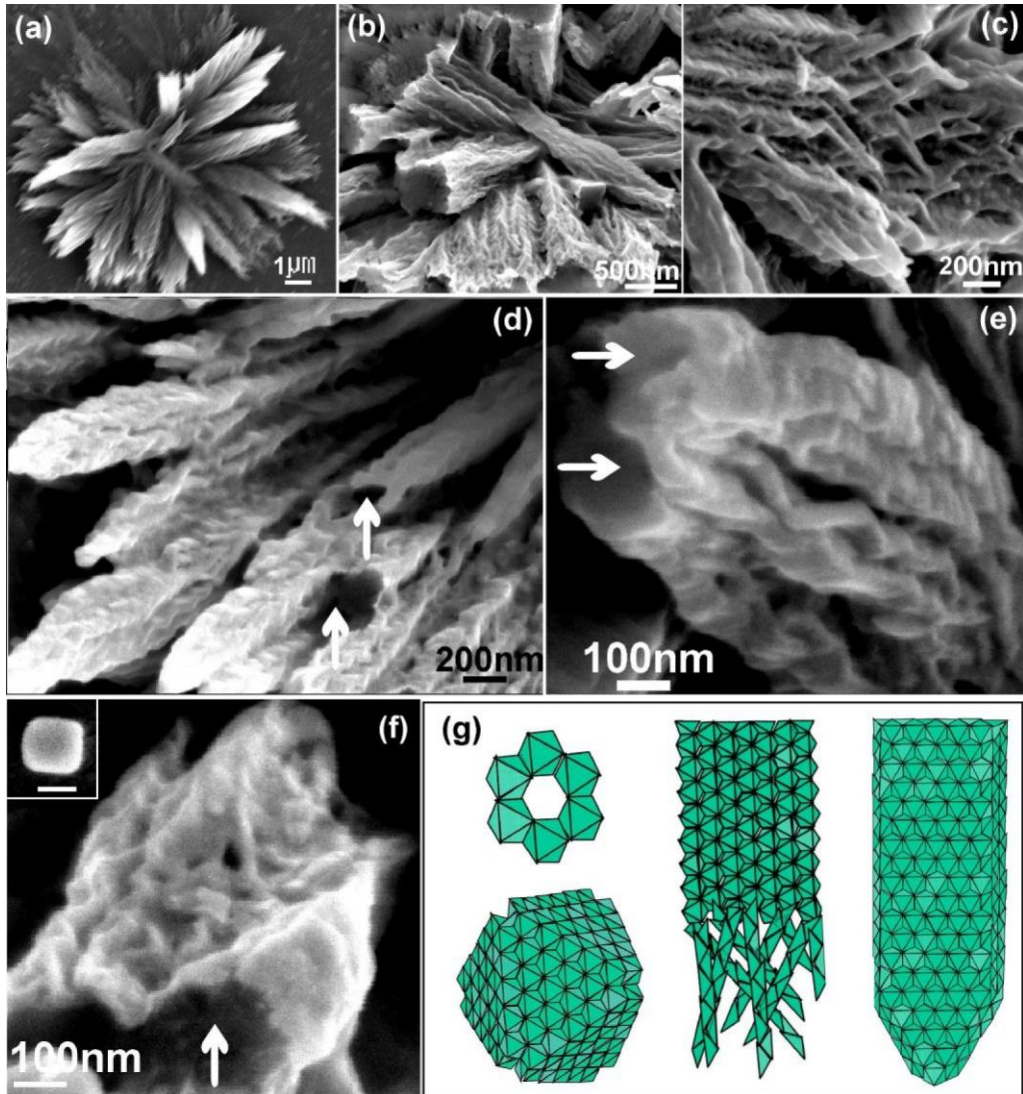


Figure. 7: (a) An individual flower exhibiting multi-fold symmetry. (Synthesis conditions: 35% ammonia solution, laser power 100 mJ, 3 h ablation and dried in a sealed tube) (b-f) Different arrangements of components construct the final hierarchical superstructures. Arrows point to the inside surface of the tubular nanopetals. Inset of Fig. 7f shows a single nanocrystal as building block, scale bar: 15 nm. (g) Schematic illustration of a suggested mechanism for the assembly of higher-order structures by nucleating new crystals through an edge sharing configuration.

In principle, assembly is energetically favored because the formation of larger crystals can greatly reduce the interfacial energy of isolated NPs or NRs. Fig. 7g summarizes a possible process for the carbon nitride self-assembly, mentioned above. By the aid of the solid substrate, hierarchically ordered nanocrystals assemble towards the surface of the substrate. New nanocrystals nucleate on the existing crystals and share the same edges. These structures are close-packed but still have spaces between them. It is still unclear why the NPs or NRs form such arrangements rather than random clumps. Further investigation of this mechanism is required.

The morphology of the self-assembled nanostructures is tuneable with the reaction conditions. By applied different building blocks, different final complex architectures on various scales can be achieved, as discussed in section 3.3. For lower ammonia concentration (25%), the carbon nitride formed 1D elongated nanoneedles or NRs. For low laser power (50 mJ) and short ablation time (2 h), the product contained mostly a sparse collection of these isolated NRs (Fig. 8a). However, with increasing laser power (125 mJ) and ablation time (10 h), the concentration of NRs increased, and in some regions they began to coalesce into incomplete flowers (Fig. 8b). The radial distribution of the NRs formed channels leading from the centre of the flower to the edge. These channels may form the conduits along which the NPs diffuse outwards. When a droplet of the suspension, identical to that shown in Fig. 8a, was deposited on the substrate and dried for 12 h in a sealed tube, the carbon nitride produced flower-like structures constructed from pronounced tapered NRs (Fig. 8c), instead of flowers made by the nanopetals (see Fig. 7a). Fig. 8d shows typical NR building blocks with a rod diameter of 10-20 nm.

A new morphology was also observed when the carbon nitride was created using a laser power of 75 mJ for 3 h ablation and placed onto a silicon substrate, and then dried in a CPD. Fig. 8e suggests that the product has a grass-like shape consisting of well-defined, protruding, short NRs. These structures can be assigned to the second class of morphology, mention previously. In contrast, if the substrate was dried in air (water evaporation time  $\sim$ 8 h), the individual NRs vertically assembled into bundles (see the highlighted black box region in Fig. 8f) and formed stem-like structures. When the

evaporation time of the liquid was increased to 24 h, the NRs developed a more complicated 3D structure, as shown in Fig. 8g.

A possible explanation is that the longer time for evaporation of liquid allows sufficient time for the diffusion of all the NPs out of the flowers, leaving some liquid trapped in the gaps between the NR framework. With prolonged time, the wet NR framework has the opportunity to recrystallise or restructure into the shapes shown in Fig. 8f-g.

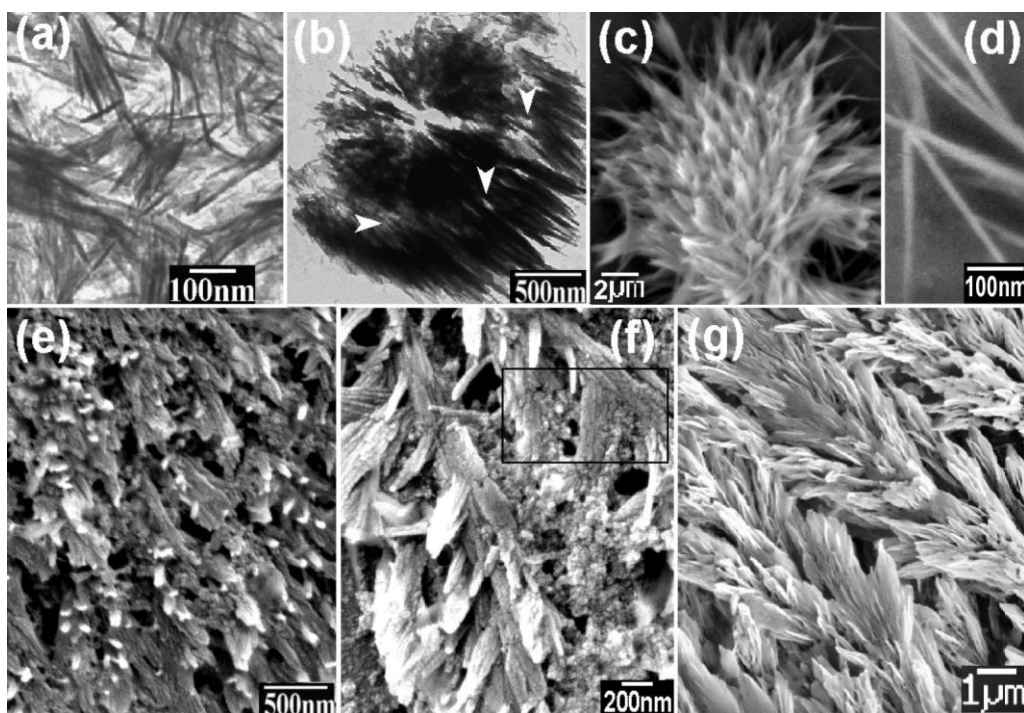


Figure. 8: (a) TEM image of isolated carbon nitride NRs obtained by LP-PLA in 25% ammonia solution (laser fluence at 50 mJ per pulse,  $t = 2$  h). (b) TEM image of an incomplete carbon nitride flower (25% ammonia solution, laser fluence at 125 mJ per pulse,  $t = 10$  h) formed by the coalesced NRs. The arrows highlight the channels between the shell and the core. (c) After drying for 12 h (sample conditions identical to that in Fig. 8a), numerous aligned NRs form the framework of the flower. (e) Grass-like structure constructed from many protruding NRs (25% ammonia solution, laser fluence at 75 mJ per pulse,  $t = 3$  h, drying at CPD). (f) Stem-like structure consisting of vertical NR branches (region highlighted by black box), sample conditions identical to that in Fig. 8e, but with drying in air. (g) After 24 h drying, the NRs have restructured to form 3D shapes. (Reproduced from [48] by the permission of RSC)

Thus, by combining LP-PLA techniques with bottom-up self-assembly seeded growth, 3D complex well-arranged carbon nitride architectures can be created, with their structures and spatial organisation of the substrate controlled by deposition and drying conditions. The synthetic approach described above can also be extended to a range of other solid materials. For example, we have also demonstrated that a novel hierarchical and self-similar growth process can happen in zinc oxide materials by LP-PLA of a zinc plate submerged in aqueous SDS solution. The growth mechanism here also appears to involve an increase of the structural complexity from 0-dimensional nanoparticles to 1-dimensional nanorods, and then broadening of these into 2-dimensional ‘nano-leaf’ structures. Details can be seen in our previous report. [75]

## 5. Conclusion

With important discoveries continuing to be made in the field of nanomaterials, fulfilling the potential applications will require a greater control of material properties, along with a better understanding of the mechanisms for nanocrystal nucleation and growth. Extensive progress towards real-life applications have been made with ZnO, Cu<sub>2</sub>O, TiO<sub>2</sub> and SiO<sub>2</sub> nanostructures, because of work on these materials is well established [70] However, research on the understanding of the self-assembly processes of Group IV-V compounds, such as carbon nitride, is still in its infancy, and synthesis of complex nanostructures has only just begun. Our work has shown that it is possible to form self-assembled nanostructures and microstructures of crystalline carbon nitride. Through pulsed laser ablation of graphite in ammonia solutions, well-defined carbon nitride nanocrystal seeds were prepared. In the second step, 3D well-arranged architectures could be generated after these solutions were seeded onto a suitable substrate. The mechanism appears to involve an increase of the structural complexity from 0D NPs to 1D NRs, and then broadening of these into 2D nanopetals, which finally coalesce to 3D flowers. Factors such as the ammonia concentration, laser energy, the reaction time and the evaporation rate of the liquid are important in defining the structures observed. This unique process provides more insight into laser-induced chemical reactions in general, and of crystalline carbon nitride phases in particular, and

may provide an alternative synthesis method for other composite nanostructures. A key advantage afforded by this aqueous multistage approach is the ability to systematically generate and control a diverse array of structures from a simple and inexpensive chemical route. With this improved understanding and concomitant seed control, LP-PLA may provide versatile and powerful industrial scale production processes for assembling complex architectures by specific design.

- 
- [1] Whitesides, G. M.; Grzybowski, B. *Science* 2002, 295, 2418-2421.
- [2] Whitesides, G. M.; Boncheva, M. *Proc. Natl Acad. Sci. USA* 2002, 99, 4769-4774.
- [3] Tang, Z. Y.; Kotov, N. A.; Giersig, M. *Science* 2002, 297, 237-240.
- [4] Liu, B.; Zeng, H.C. *J. Am. Chem. Soc.* 2005, 127, 18262-18268.
- [5] Kempa, K.; Kimball, B.; Rybczynski, J.; Huang, Z. P.; Wu, P. F.; Steeves, D.; Sennett, M.; Giersig, M.; Rao, D. V. G. L. N.; Carnahan, D. L.; Wang, D. Z.; Lao, J. Y.; Li, W. Z.; Ren, Z. F. *Nano Lett.* 2003, 3, 13-18.
- [6] Duan, X. F.; Lieber, C. M. *Adv. Mater.* 2000, 12, 298-302.
- [7] Sun, Y.; Fuge, G. M.; Fox, N. A.; Riley, D. J.; Ashfold, M. N. R. *Adv. Mater.* 2005, 17 2477-2480.
- [8] Yang, H. G.; Zeng, H. C. *J. Phys. Chem. B* 2004, 108, 3492-3495.
- [9] Mirkin, C. A.; Letsinger, R. L.; Mucic, R. C.; Storhoff, J. J. *Nature* 1996, 382, 607-609.
- [10] Sun, Y. G.; Gates, B.; Mayers, B.; Xia, Y. N. *Nano Lett.* 2002, 2, 165-168.
- [11] Li, Y.D.; Li, X. L.; Deng, Z. X.; Zhou, B. C.; Fan, S. S.; Wang, J. W.; Sun, X. M. *Angew. Chem. Int. Ed.* 2002, 41, 333-335.
- [12] Motte, L.; Billoudet, F.; Pileni, M. P. *J. Phys. Chem.* 1995, 99, 16425-16429.
- [13] Maillard, M.; Motte, L.; Pileni, M. P. *Adv. Mater.* 2001, 13, 200-204.
- [14] Liu, B.; Zeng, H.C. *J. Am. Chem. Soc.* 2004, 126, 16744-16746.
- [15] Petit, C.; Legrand, J.; Russier, V.; Pileni, M. P. *J. Appl. Phys.* 2002, 91, 1502-1508.
- [16] Ngo, A. T.; Pileni, M. P. *Adv. Mater.* 2000, 12, 276-279.
- [17] Liu, J. P.; Huang, X. T.; Li, Y. Y.; Sulieman, K. M.; He, X.; Sun, F. L. *J. Mater. Chem.* 2006, 16, 4427-4434.
- [18] Wang, J. B.; Zhang, C. Y.; Zhong, X. L.; Yang, G. W. *Chem. Phys. Lett.* 2002, 361, 86-90.

- 
- [19] Dijkkamp, D.; Venkatesan, T.; Wu, X. D.; Shaheen, S. A.; Jisrawi, N.; Minlee, Y. H.; Mclean, W. L.; Croft, M. *Appl. Phys. Lett.* 1987, *51*, 619-621.
- [20] Radhakrishnan, G.; Adams, P. M. *Appl. Phys. A* 1999, *69*, S33-S38.
- [21] Pappas, D. L.; Saenger, K. L.; Bruley, J.; Krakow, W.; Cuomo, J. J.; Gu, T.; Collins, R. W. *J. Appl. Phys.*, 1992, *71*, 5675-5864.
- [22] Loir, A. S.; Garrelie, F.; Donnet, C.; Belin, M.; Forest, B.; Rogemond, F.; Laporte, P. *Thin Solid Films*, 2004, *453*, 531-536.
- [23] Patil, P. P.; Phase, D. M.; Kulkarni, S. A.; Ghaisas, S. V.; Kulkarni, S. K.; Kanetkar, S. M.; Ogale, S. B.; Bhide, V. G. *Phys. Rev. Lett.*, 1987, *58*, 238-241.
- [24] Ogale, S. B. *Thin Solid Films* 1988, *163*, 215-227.
- [25] Yang, G. W. *J Prog. Mater. Sci.* 2007, *52*, 648-698.
- [26] Pyatenko, A.; Shimokawa, K.; Yamaguchi, M.; Nishimura, O.; Suzuki, M. *Appl. Phys. A*. 2004, *79*, 803-806.
- [27] Tsuji, T.; Iryo, K.; Watanabe, N.; Tsuji, M.; *Appl. Surf. Sci.* 2002, *202*, 80-85.
- [28] Dolgaev, S. I.; Simakin, A.V.; Voronov, V. V.; Shafeev, G. A.; Bozon-Verduraz, F. *Appl. Surf. Sci.* 2002, *186*, 546-551.
- [29] Tarasenko, N. V.; Butsen, A. V.; Nevar, E. A.; Savastenko, N. A. *Appl. Surf. Sci.* 2006, *252*, 4439-4444.
- [30] Compagnini, G.; Scalisi, A. A.; Puglisi, O. *J. Appl. Phys.* 2003, *94*, 7874-7877.
- [31] Tsuji, T.; Hamagami, T.; Kawamura, T.; Yamaki, J.; Tsuji, M. *Appl. Surf. Sci.* 2005, *243*, 214-219.
- [32] Wang, J. B.; Zhang, C. Y.; Zhong, X. L.; Yang, G. W. *Chem. Phys. Lett.* 2003, *367*, 10-14.

- 
- [33] Yang, G. W.; Wang, J. B.; *Appl. Phys. A* 2000, *71*, 343-344.
- [34] Wang, J. B.; Zhang, C. Y.; Zhong, X. L.; Yang, G. W. *Chem. Phys. Lett.* 2002, *361*, 86-90.
- [35] Yang, L.; May, P. W.; Yin, L.; J. A.; Rosser, K. N. *Diamond Relat. Mater.* 2007, DOI:10.1016/j.diamond.2006.11.010
- [36] Nath, M.; Rao, C. N. R.; Popvitz-biro, R.; Albu-Yaron, A.; Tenne, R. *Chem. Mater.* 2004, *16*, 2238-2243.
- [37] Liang, C. H.; Sasaki, T.; Shimizu, Y.; Koshizaki, N. *Chem. Phys. Lett.* 2004, *389*, 58-63.
- [38] Sasaki, T.; Liang, C. H.; Nichols, W. T.; Shimizu, Y.; Koshizaki, N. *Appl. Phys. A* 2004, *79*, 1489.
- [39] Liang, C. H.; Shimizu, Y.; Sasaki, T.; Koshizaki, N. *J. Phys. Chem. B* 2003, *107*, 9220-9225.
- [40] Liang, C. H.; Shimizu, Y.; Sasaki, T.; Koshizaki, N. *Appl. Phys. A* 2005, *80*, 819-822.
- [41] Liang, C. H.; Shimizu, Y.; Sasaki, T.; Koshizaki, N. *J. Mater. Res.* 2004, *19*, 1551-1557.
- [42] Zeng, H. B.; Cai, W. P.; Li, Y.; Hu, J. L.; Liu, P. S. *J. Phys. Chem. B* 2005, *109*, 18260-18266.
- [43] Ishikawa, Y.; Shimizu, Y.; Sasaki, T.; Koshizaki, N. *J. Colloid Interf. Sci.* 2006, *300*, 612-615.
- [44] Usui, H.; Sasaki, T.; Koshizaki, N. *Appl. Phys. Lett.* 2005, *87*, 063105-3.

- 
- [45] Yang, L.; May, P. W.; Yin, L.; Brown, R.; Scott, T. B. *Chem. Mater.* 2006, *18*, 5058-5064.
- [46] Yang, L.; May, P. W.; Yin, L.; J. A.; Rosser, K. N. *J. Nanopart. Res.* 2007, DOI 10.1007/s11051-006-9192-4.
- [47] Liu, A. Y.; Cohen, M. L. *Science* 1989, *245*, 841-842.
- [48] Yang, L.; May, P. W.; Huang, Y. Z.; Yin, L. *J. Mater. Chem.* 2007, DOI: 10.1039/b701914a
- [49] Yang, L.; May, P. W.; Yin, L.; Scott, T. B.; Smith, J. A.; Rosser, K. N. *Nanotechnology* 2006, *17*, 5798-5804.
- [50] Liu, A.Y.; Wentzcovitch, R. M. *Phys. Rev. B* 1994, *50*, 10362-10365.
- [51] Wang, J. B.; Lei, J. L.; Wang, R. H. *Phys. Rev. B* 1998, *58*, 11890-11895.
- [52] Yin, L. W.; Bando, Y.; Li, M. S.; Liu, Y. X.; Qi, Y. X. *Adv. Mater.* 2003, *15*, 1840-1844.
- [53] Zeng, H.C. *J. Mater. Chem.* 2006, *16*, 649-662.
- [54] Sjöström, H.; Staftröm, S.; Boman, M.; Sundgren, J. E. *Phys. Rev. Lett.* 1995, *75* 1336-1339.
- [55] Terrones, M.; Redlich, P.; Grobert, N.; Trasobares, S.; Hsu, W. K.; Terrones, H.; Zhu, Y. Q.; Hare, J. P.; Reeves, C. L.; Cheetham, A. K.; Rühle, M.; Kroto, H. W.; Walton, D. R. M. *Adv. Mater.* 1999, *11*, 655-658.
- [56] Rodil, S. E.; Muhl, S. *Diamond Relat. Mater.* 2004, *13*, 1521-1531.
- [57] Hellgren, N.; Johansson, M. P.; Broitman, E.; Hultman, L.; Sundgren, J. E. *Phys. Rev. B* 1999, *59*, 5162-5169.
- [58] Muhl, S.; Méndez, J. M. *Diamond Relat. Mater.* 1999, *8*, 1809-1830.

- 
- [59] Hellgren, N.; Guo, J.; S athe, C.; Agui, A.; Nordgren, J.; Luo, Y.;  gren, H.; Sundgren, J. *Appl. Phys. Lett.* 2001, *79*, 4368-4350.
- [60] Souto, S.; Pickholz, M.; Dos Santos, M. C.; Alvarez, F. *Phys. Rev. B* 1998, *57*, 2536-2540.
- [61] Ripalda, J. M.; Montero, I.; Galan, L. *Diamond Relat. Mater.* 1998, *7*, 402-406 .
- [62] Ogata, K.; Chubaci, J. F. D.; Fujimoto, F. *J. Appl. Phys.* 1994, *76*, 3791-3796.
- [63] Khabashesku, V. N.; Zimmerman, J. L.; Margrave, J. L. *Chem. Mater.* 2000, *12*, 3264-3270.
- [64] Diaz, J.; Paolicelli, G.; Ferrer, S.; Comin, F. *Phys. Rev. B* 1996, *54*, 8064-8069.
- [65] Tabbal, M.; Merel, P.; Moisa, S.; Chaker, M.; Ricard, A.; Moisan, M. *Appl. Phys. Lett.* 1996, *69*, 1698-1700.
- [66] Le Normand, F.; Hommet, J.; Sz orenyi, T.; Fuchs, C.; Fogarassy, E. *Phys. Rev. B* 2001, *64*, 235416-15.
- [67] Beamson, G.; Briggs, D.; *High Resolution XPS of Organic Polymers*; 1992, John Wiley and Sons, Chichester, pp.182.
- [68] Guo Y. J.; Goddard, W.A. *Chem. Phys. Lett.*, 1995, *237*, 72-76.
- [69] Niesen, T. P.; De Guire, M.R. *J. Electroceram.* 2001, *6*, 169-207.
- [70] Sounart, T. L.; Liu, J.; Voigt, J. A.; Hsu, J. W. P.; Spuerke, E. D.; Tian, Z.; Jiang, Y. B. *Adv. Funct. Mater.* 2006, *16*, 334-344.
- [71] Lu, S.N; Chung, J.; Ruoff, R.S. *Nanotechnology* 2005, *16*, 1765-1770.
- [72] Brinker, C. J.; Lu, Y. F.; Sellinger, A.; Fan, H. Y. *Adv. Mater.* 1999, *11*, 579-585.
- [73] Liu, A. Y.; Cohen, M. L. *Phys. Rev. B* 1990, *41*, 10727-10734.
- [74] Li, Z. Q.; Xiong, Y. J.; Xie, Y. *Nanotechnology* 2005, *16*, 2303-2308.

---

[75] Yang, L.; May, P. W.; Yin, L. *Nanotechnology*, 2007, under review.